Blood-tumor barrier organoids recapitulate glioblastoma microenvironment and enable high-throughput modeling of therapeutic delivery

Pei Zhuang[1], Benjamin Scott[1], Shuai Gao[1], Wei-Min Meng[2], Rui Yin[2], Xinyu Nie[1], Ludovica Gaiaschi[1,3], Sean E. Lawler[4], Martine Lamfers[5], Fengfeng Bei[1], Choi-Fong Cho[1,6,7,8,*]

[1]Department of Neurosurgery, Brigham and Women's Hospital, Harvard Medical School, Boston, Massachusetts 02115, USA.
[2]Department of Health Outcomes and Biomedical Informatics, University of Florida, Gainesville, FL 32611, USA
[3]Laboratory of Cell Biology and Neurobiology, Department of Biology and Biotechnology "L. Spallanzani", University of Pavia, Via Ferrata 9, 27100 Pavia, Italy
[4]Department of Pathology and Laboratory Medicine, Legorreta Cancer Center, Brown University, Providence, RI 02903, USA
[5]Department of Neurosurgery, Brain Tumor Center, Erasmus Medical Center, Dr. Molewaterplein 40, 3015 GD Rotterdam, the Netherlands
[6]Program in Neuroscience, Harvard Medical School, Boston, MA 02115, United States.
[7]Harvard Stem Cell Institute, Harvard University, Boston, MA 02115, United States.
[8]Dana-Farber Harvard Cancer Center, Boston, MA 02115, United States.

*Correspondence: ccho@bwh.harvard.edu

The blood-brain barrier (BBB) is a highly specialized system that is critical for regulating transport between the blood and the central nervous system. In brain tumors, the vasculature system is compromised, and is referred to as the blood-tumor barrier (BTB). The ability to precisely model the unique physiological properties of the BTB is essential to decipher its role in tumor pathophysiology and for the rational design of efficacious therapeutics. Here, we introduce a robust and high-throughput *in vitro* 3D human BTB organoid model that recapitulates various key features of the BTB observed *in vivo* and in clinical GBM samples. The organoids are composed of patient-derived glioblastoma stem cells (GSCs), human brain endothelial cells (EC), astrocytes and pericytes, which are formed through self-assembly. Transcriptomic and functional analyses reveal that the GSCs in the BTB organoids exhibit enhanced level of stemness, mesenchymal signature, invasiveness and angiogenesis, and this is further confirmed in *in vivo* studies. We demonstrate the ability of the BTB organoids to model therapeutic delivery and drug efficacy on brain tumor cells. Collectively, our findings show that the BTB organoid model has broad utility as a clinically representative system for studying the BTB and evaluating brain tumor therapies.

Introduction

Despite significant advancements in cancer research, malignant brain tumors including glioblastoma (GBM) remain a formidable challenge in both adults and children[1]. The standard-of-care for GBM (maximal surgical resection, followed by radio-chemotherapy) and alternative treatments such as immunotherapy have been extensively investigated, yet patients often face disease relapse[2]. A major stumbling block for effective therapeutic development for brain tumors is the presence of the blood-brain barrier (BBB) that hinders drug delivery to tumor sites[3]. The BBB features a unique and intricate structural arrangement of the neurovascular unit (NVU), primarily composed of tightly connected EC that are closely associated with astrocytes, pericytes, neurons and other cell types, which are critical for maintaining barrier integrity[4]. Tumor cells co-opt the CNS microvasculature for a continuous supply of oxygen, nutrients and growth factors for sustained propagation. The brain tumor vasculature is altered, forming the blood-tumor-barrier (BTB) consisting of both fenestrated (leaky) and non-fenestrated endothelia that are heterogeneously permeable to various therapeutics, contributing to poor treatment efficacy. The complex and highly

dynamic interaction and mechanisms between the tumor cells and surrounding NVU remain to be fully understood[5,6].

Neuro-oncology research heavily depends on animal models. Major challenges associated with *in vivo* models include high variability in engraftment efficiency, interspecies differences, low throughput, labor intensiveness and time consumption with some tumors taking months to establish[7]. *In vitro* BTB models that can recapitulate the features of brain tumor cells and their associated vasculature with high fidelity are crucial for understanding the tumor biology and predicting therapeutic efficacy prior to conducting costly and laborious *in vivo* studies. *In vitro* culture models including cancer cell lines and glioma stem cell (GSC) neurospheres are often used as a starting point, providing valuable information to complement *in vivo* findings[8]. To date, relatively few studies have included tumor cells in BBB culture models *in vitro*[6], exacerbating the gap in our understanding of BTB dynamics. Most widely described *in vitro* BTB systems involve the 2D transwell model, where brain EC (along with other NVU cells) are typically cultured on a semiporous membrane on the upper apical side, while GBM cells are cultured in the lower basal chamber[9,10], allowing exposure of all cells to the condition media without being in direct contact. Despite its prevalence owing to easy accessibility and versatility, the transwell model has several well-known limitations including the inability to faithfully represent the complex 3D microenvironment of the BTB and account for direct cell-cell interactions which are known to be critical for tumor plasticity. The development of vascularized 3D microfluidic-based BTB chips offer more accurate simulations of the BTB microenvironment[11]. However, microfluidic platforms provide limited scalability and require specialized equipment to construct which can be technically challenging, making them relatively less accessible to the scientific community.

We have previously described a human BBB organoid model that reproduces key BBB marker expression and functions, as well as predicts BBB permeability *in vivo*[12–18]. The BBB organoids are formed through the self-assembly of a co-culture of human NVU cells: Human brain EC encase the organoid outer surface together with associating human brain pericytes, while the core consists mostly of human astrocytes. Here, we demonstrate for the first time, the incorporation of GSC into the BBB organoid platform to give rise to a novel BTB organoid model. Comprehensive structural, genetic and functional characterization shows that this model recapitulates tumor neovascularization processes and significant oncogenic features observed in GBM patient samples, including enhanced stemness, aggressiveness, angiogenesis and extracellular matrix (ECM) remodeling compared to the corresponding GSC monocultures. We further demonstrate the utility of the BTB organoids for modeling therapeutic delivery to GBM cells using a known GBM-targeting peptide (BTP-7) and a BBB-penetrating adeno-associated virus (AAV.CPP.16) as proofs-of-concept[14,16,18], highlighting the predictive capability and value of the BTB organoid platform for drug development.

Results

Establishing the BTB organoids

The BTB organoid was formed through the self-organization of a mixture of cells comprising patient-derived GSC, human cerebral microvascular endothelial cells (hCMEC), human brain vascular pericytes (HBVP) and human astrocytes (HA) in co-culture. Immunofluorescence staining of cell-specific biomarkers confirmed the identity of the HBVP through PDGFR-β expression, HA through glial fibrillary acidic protein (GFAP) expression, and hCMEC through CD31 and CD105 expression (**Figure S1A**)[12,13].

GSCs are normally maintained in the absence of serum in Neurobasal (NB) media to preserve their stem-like state[19]. GSCs cultured in media containing 10% fetal bovine serum (FBS) have been reported to lose their stem-like properties over time to become vastly different from their parental tumor genetic profile[19,20]. The BBB organoids are typically cultured in endothelial basal media containing 1.5% human serum (HS)[21,22]. To establish an integrated co-culture condition, our early studies sought to examine the effects of 1.5% HS on GSC stemness.

The BTB organoids were formed through the co-culture of HA, HBVP, and hCMEC and GSCs in the presence of either 1.5% human serum (HS) or serum-free (NB) conditions for 72 h. We used 5 human GSC models to demonstrate our approach – G9, G30, GBM-X6, GS184 and GS401 (the latter 3 GSCs are derived from GBM patients). GS184 and GS401 are paired tumor cells obtained from the same patient at the primary and recurrence disease stage, respectively. We observed that each GSC exhibited distinct characteristics in the BTB organoids (**Figure S1B**). For example, in HS condition, GS184 (primary) cells had the tendency to form compact tumor clumps, while GS401 (recurrent) cells were more infiltrative and dispersed throughout the organoid. In all cases, the GSCs were initially embedded within the organoid, then began to proliferate and invade into the surrounding microenvironment and toward the organoid surface over time. The BTB organoids were larger (300-400 µm diameter) than the BBB organoids (200-300 µm diameter), and they continued to be viable over several weeks.

Immunofluorescence staining and flow cytometry analysis revealed stable expression of canonical stem cell markers – Sox2, Nestin and Olig2 in the GSCs after 72 h of culture in both NB and HS conditions, confirming the preservation of their stem-like state in HS condition **(Figure 1A, 1B, and S1C, S1D)**. All GSCs in both BTB organoids and monocultures showed increased proliferation rate in HS condition compared to NB (**Figure 1D, S1E**).

To investigate the cellular arrangement within the BTB organoid, each cell type was labeled as follows: HBVP (pre-labeled with CellTracker Green), HA (pre-labeled with CellTracker Violet), hCMEC (express red fluorescent protein (RFP)), and GSCs (stained for Nestin expression). In the absence of tumor cells in the BBB organoids, hCMEC and associated HBVP predominantly lined the outer surface, characterized by the expression of a high level of tight junctions along with other BBB markers, while HA occupied the core[21]. In the BTB organoids, the invasive GSCs caused major structural reorganization between all cell types and disruption of the tight endothelial lining on the organoid surface (**Figure 1C**). We also noted that HA cells had the tendency to rearrange themselves in proximity to the GSCs to form tightly-associated clusters (**Figure 1C**). This phenomenon is reminiscent of reactive astrocytes that have been identified to be closely associated with GBM tissues[23].Though the function of reactive astrocyte is not fully understood, accumulating evidence have suggested a pivotal role in supporting GBM progression, invasion and migration[24], suppressing immune responses[23], and enhancing resistance to chemoradiotherapy[25,26].

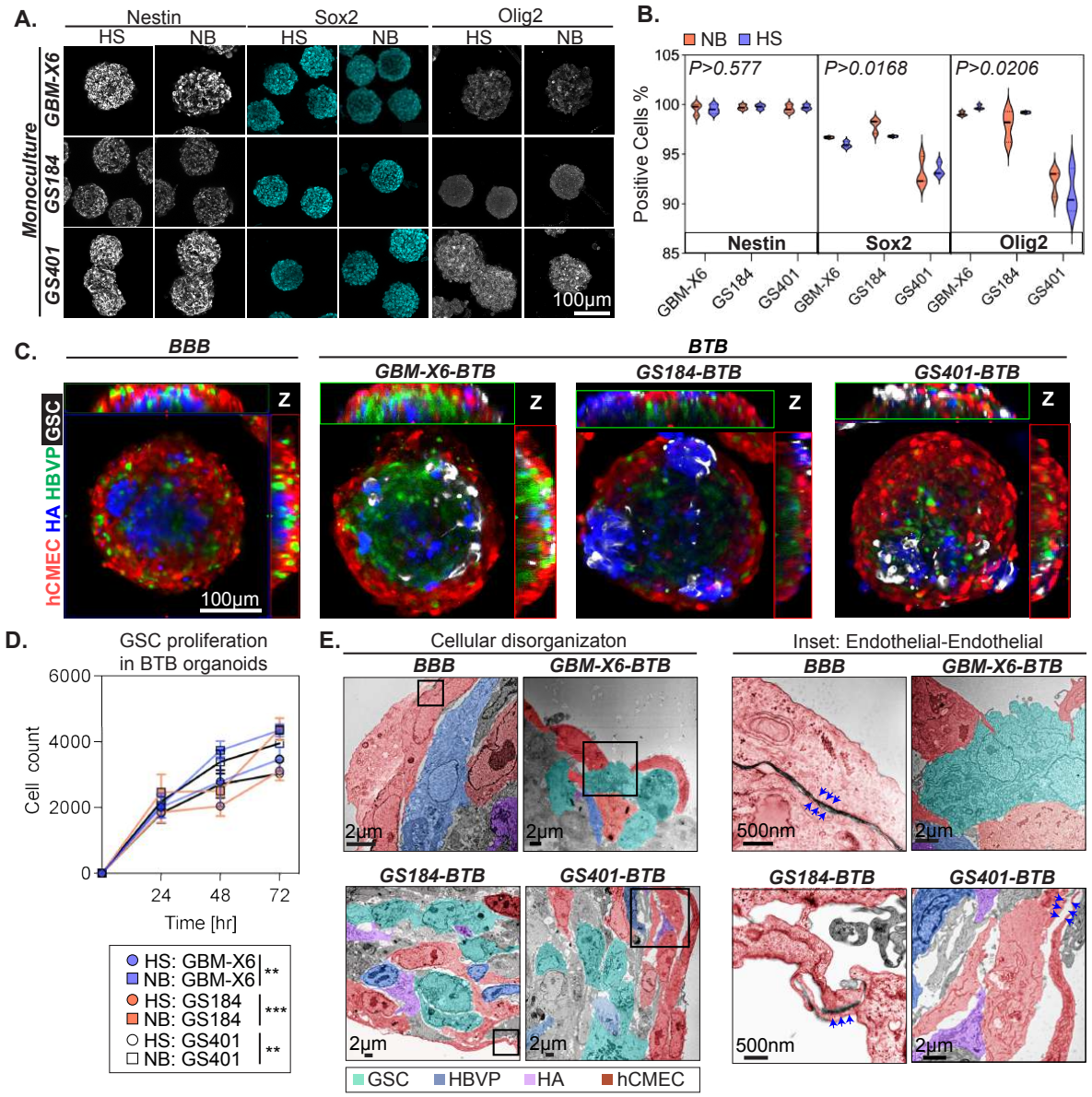

Figure 1. Blood-tumor barrier (BTB) organoid formation and structural organization.

(A) Representative confocal images showing the expression of the canonical stem cell markers (Sox2, Nestin and Olig2) in GSC monocultures following a 72-h culture in HS or NB condition. Scale bar, 100 µm.

(B) Quantification of Sox2-, Nestin- and Olig2-positive GSCs in HS or NB culture conditions from flow cytometry analysis in Figure S1C.

(C) Representative confocal images depicting the cellular organization of the BBB and BTB organoids. In the BBB organoids, the brain endothelial cells (red) encase the outer surface with associated HBVP (green), with an astrocytic (blue) core. The BTB organoids display a notable structural rearrangement, such as reorganization of HA cells in proximity to the GSCs (white). Scale bar, 100 µm.

(D) Proliferation rate of the GSCs in BTB organoids in HS and NB culture conditions. GSCs have higher proliferation rates in HS relative to NB across all groups (n = 3 each group, mean ± s.d., two-way ANOVA with Sidak's multiple comparison test, **P < 0.01, ***P < 0.001).

(E) Representative TEM images displaying the cellular organization in the BBB and BTB organoids. The cell types are distinguished using different colors. The magnified insets (right panels) show the formation of intact tight junctions (blue arrows) between adjacent brain endothelial cells in the BBB organoids, while the tight junctions in the BTB organoids appear disrupted or truncated. Scale bar is specified in each image.

We further conducted transmission electron microscopy (TEM) analyses to gain deeper insight into the ultrastructure of the BTB organoids. Each cell type of the NVU was identified through specific TEM features as previously described[21] and demonstrated in **Figure S1F**. The GSCs typically feature polymorphic and convoluted nuclei **(Figure S1G-a,** blue**),** breakdown of cristae in mitochondria across the GBM cells (green arrow) **(Figure S1G-b),** Golgi apparatus (**Figure S1G-c**, red arrow), abundant intermediate cytoplasmic filaments and vesicles (**Figure S1G-c**). Consistent with our immunofluorescence imaging findings, the presence of GSCs resulted in significant disruption in the structural organization of the BTB organoids compared with the BBB organoids, and a marked decrease and disruption of tight junctions on the endothelial surface (**Figure 1E**).

Permeability in BTB organoids

As GBM lesions continue to grow, they undergo various neovascularization processes such as vascular angiogenesis and co-option to ensure a continuous blood supply[27]. These processes lead to the formation of tortuous and dilated vessels, which directly affect vascular permeability, resulting in 'leaky' barriers compared to the healthy BBB. To investigate the effect of GSCs on BTB organoid permeability, we evaluated the influx of TRITC-dextran. The initial cell count for each GSC sphere within a range of 50-1000 cells was tailored to their own growth kinetics as monocultures.

We have previously established that the surface of BBB organoids is impermeable to TRITC-dextran[21,22]. In the BTB organoids, higher level of TRITC-dextran influx was observed in a cell density-dependent manner compared to the BBB organoids (no GSC), suggesting disruption of BBB function by the tumor cells leading to increased leakiness and permeability **(Figure 2A, Figure S2B**). This increase in dextran influx was exacerbated in HS condition compared to NB (**Figure 2A, Figure S2B**), likely attributed to the higher proliferation rate of the GSCs in HS. In some cases, an uneven distribution of dextran in the BTB organoid was observed (**Figure S2A**), where higher level of TRITC signal was detected near the tumor mass, further linking the cause of barrier leakiness to the GSCs.

To study the importance of direct cell-cell interaction between the tumor and NVU cells for modeling BBB disruption, we exposed BBB organoids to GSC conditioned medium, which was produced by culturing 20,000 GSCs in 1 mL of media supplemented with 1.5% HS, representing a cell density more than 40 times higher than that utilized in the BTB model. Only a modest to no increase in dextran influx was observed in GSC conditioned media even after 72 h (**Figure 2B, S2C**). This is in contrast to the significant leakiness seen in the BTB organoids, for example, GS401-BTB organoids containing fewer than 1000 cells exhibited more than a two-fold increase in dextran influx (**Figure 2A**). These results underscore the vital role of direct cell-cell contact for modeling BTB events.

The physical proximity of GSC and EC has been reported to create a localized perivascular niche where their interactions regulate GSC stemness, migration, therapy resistance and tumor dynamics[28]. In the BTB

organoids, the GSCs and EC exhibited highly dynamic interactions as seen using time-lapse confocal microscopy. Single ECs were observed to adopt an elongated spindle-shaped morphology as they migrated towards and invaded into the tumor mass (**Figure S2D, Supplementary video 1, 2, 3, 5**), a phenomenon that resembles tube formation during the process of angiogenesis.

Disruption of barrier integrity by GSCs

The restrictive property of the BBB is determined by junctional complexes formed between neighboring brain EC, including tight, adherens, and gap junctions. We observed a decrease in ZO-1 expression on the BTB organoid surface which correlated with increasing GSC cell count, indicating tight junction disruption by the GSCs (**Figure 2C, 2D, S2E**). Similarly, the expression of another tight junction protein, Claudin-5 was decreased in the BTB organoids compared to the control BBB organoids (**Figure 2E**). The expression of VE-cadherin, which plays a vital role in adherens junction assembly and vascular permeability[29], was also significantly reduced in the BTB organoids compared to the BBB organoids (**Figure 2F**, **I).** These findings point to the various alterations in junctional protein expression caused by the tumor cells, compromising the cell-cell junction stability on the organoid surface that would lead to increased barrier leakage.

The lipid transporter Mfsd2a (major facilitator super family domain containing 2a) is known to suppress caveolae-mediated transcytosis and is critical for the maintenance of BBB integrity[30]. Immunofluorescence staining of the BTB organoids showed a marked decrease in Mfsd2a expression compared to the BBB organoids (**Figure 2G, J**), indicating that the tumor cells can promote transcytosis in the surrounding brain EC. This phenomenon is consistent with *in vivo* observations, where a loss of Mfsd2a expression in the tumor endothelium leading to enhanced BBB permeability has been reported[31]. As the main glucose transporter in ECs, Glucose Transporter 1 (Glut1) is expressed abundantly on brain EC and serves as a marker of the normal BBB[32]. In the presence of GSC, we observed a reduction in Glut1 protein expression on the EC of BTB organoids (**Figure 2H, K**). This finding is in line with previous studies showing that despite increased glycolytic metabolism in GBM, the microvessels associated with malignant brain tumors exhibit low Glut1 expression compared to the normal BBB[33,34].

Even though the BTB exhibits increased 'leakiness', the delivery of efficacious levels of drug to tumor cells is often unachieved. This limitation can be largely attributed to the presence of efflux pumps, which is a major contributor to multidrug resistance[35]. P-glycoprotein (P-gp) is one of the most highly expressed efflux pumps on the BBB endothelium and is associated with cancer chemoresistance[12,36]. Indeed, we found high expression of P-gp in the BTB organoids (**Figure S2F**).

Genetic profiling of brain EC in BTB organoids

Transcriptomic analyses were performed to profile the endothelial population isolated from the BBB organoids (EC_{BBB}), GS184-BTB and GS401-BTB organoids (EC_{184} and EC_{401}) using bulk RNA sequencing. First, we compared the EC_{BBB} with a recently published study[37], which has surveyed the global gene expression profile of 109 samples across 22 libraries, including induced pluripotent stem cells (iPSC)-derived brain EC, primary endothelial (adult, fetal and human pluripotent stem cell (hPSC)-derived EC) and epithelial cells, and choroid plexus organoids. Our analysis demonstrated that the EC_{BBB} population retained

a distinct endothelial identity with minimal epithelial characteristics (**Figure S2G**), further validating the BBB properties of the organoid model.

Next, we profiled the genetic changes in the BTB organoids and observed a downregulation in several tight junction/adherens junction-associated genes, such as *TJP1*, *CLDN5*, *JAM2*, *CDH5*, *PECAM1* and *ESAM* in the EC_{BTB} population compared to the control EC_{BBB} (**Figure 2L***)*. Downregulation of *MFSD2A* was also observed (**Figure 2L**), consistent with our immunofluorescence staining findings showing a decrease in Mfsd2a protein expression (**Figure 2J**). Mfsd2a functions to suppress caveolae-mediated transcytosis, and loss of Mfsd2a leads to an upregulation of caveolae vesicle trafficking[30]. Indeed, in the EC_{BTB}, we observed an upregulation of the integral membrane proteins, caveolin-1 (*Cav1)* and caveolin-2 (*Cav2)* (**Figure 2L**), which play major roles in maintaining barrier integrity through caveolae-mediated transcytosis. To maintain normal brain function, brain EC also express various transporters, including solute carrier transporters (SLCs) for the delivery of essential nutrients, as well as efflux pumps (ABCs) for shuttling molecules back into the bloodstream[38]. In the EC_{BTB}, several SLC transporters implicated in the metabolic alterations of GBM processes were upregulated, including nucleobase transporter *SLC43A3*[39], monocarboxylate transporter *SLC16A1*[40], large neutral amino acids transporter *SLC7A5*[41], and ABC transporters (*ABCA1)* that are involved in augmenting chemoresistance to therapeutics such as temozolomide and cisplatin[42,43] **(Figure 2L)**. Indeed, elevated expression of these transporters in the GBM vasculature and their roles in promoting GBM progression and chemoresistance have been described[34].

Upregulation of the cell adhesion molecules ICAM1 and VCAM1, which mediate leukocyte recruitment, were observed in the EC_{BTB} (**Figure 2L**), indicative of neuroinflammation characterized by enhanced endothelial activation and increased BBB permeability[44]. This was accompanied by an upregulation of several inflammatory cytokines, including IL-1, TNF-α, IL-6, and CCL2.

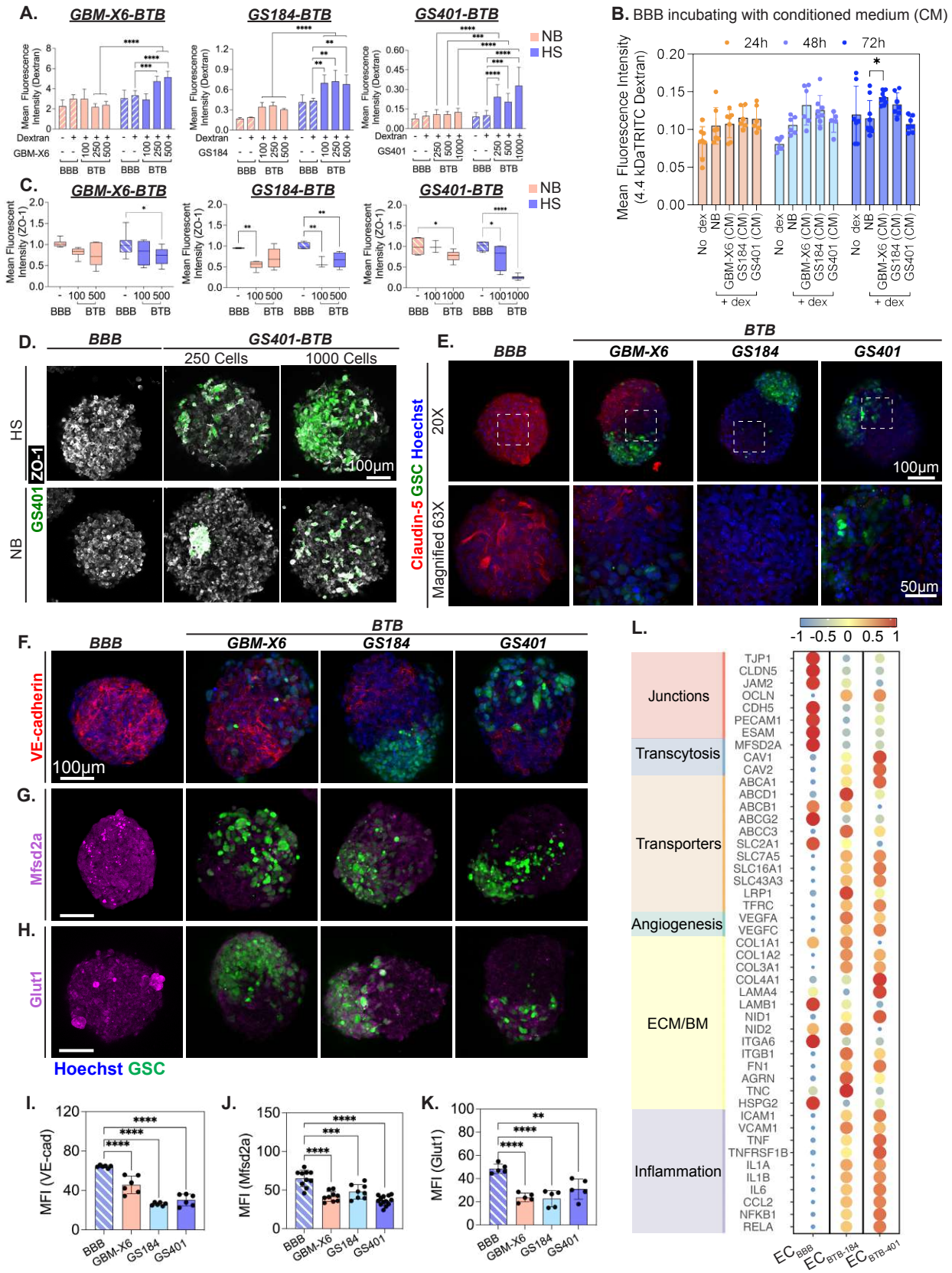

Figure 2. Dextran permeability and disruption of barrier integrity in BTB organoids.

(A) Bar graphs showing the influx of TRITC-dextran (4.4 kDa, 10 μg/mL) into the BTB organoids in a GSC density-dependent manner in HS or NB conditions (n = 6-8). Data are represented as mean fluorescence ± s.d (two-way ANOVA with Tukey's multiple comparison test, **P < 0.01, ***P < 0.001, ****P < 0.0001)
(B) Bar graph depicting the permeability of BBB organoids to dextran (4.4 kDa, 10 μg/mL) following exposure to GSC-conditioned medium for up to 72 h (two-way ANOVA with Dunnett's multiple comparisons test, **P < 0.01, ***P < 0.001, ****P < 0.0001).
(C) Mean fluorescence intensity of ZO-1 expression on the brain endothelial cells in the BBB and BTB organoids (from Figure 2D and Figure S2E) (n = 6-8).
(D) Representative confocal images showing the expression of junction marker, ZO-1 (white) from immunofluorescence staining of the BBB and GS401-BTB organoids with varying GSC (green) count. Scale bar, 100 μm.
(E) Representative confocal images showing a decrease in Claudin-5 (red) expression in the BTB organoids compared to BBB organoids. GSCs are pre-labeled with CellTracker Green. Nuclei of organoids are stained with Hoechst dye (blue). Scale bar, 100 μm in lower-magnification images (top) and 50 μm in 63x magnified insets (bottom). Representative confocal images showing the expression of **(F)** VE-cadherin (red); **(G)** Mfsd2a (magenta); **(H)** Glut1 (magenta) in the BTB and BBB organoids. Scale bar, 100 μm.
(I, J, K) Quantification of mean fluorescence intensity from the images in F, G and H, respectively. Data are represented as mean ± s.d. (one-way ANOVA with Dunnett's multiple comparisons test, **P < 0.01, ****P < 0.0001).
(L) Gene expression of brain ECs isolated from BBB (EC_{BBB}), GS184-BTB ($EC_{BTB-184}$), and GS401-BTB ($EC_{BTB-401}$) organoids. The selected genes are related to junctions, transcytosis, transporters, angiogenesis, ECM/BM and inflammation.

GSC_{BTB} display increased invasiveness and mesenchymal gene signature

To assess the effect between the GSCs and EC, bulk transcriptomic analyses of GS184, GS401, and EC in the BTB organoids were performed by RNA-sequencing. First, the GSC and EC populations were separated from HA and HBVP by fluorescence-activated cell sorting (FACS) based on the low PDGFRβ expression in the GSCs and EC (**Figure S3A**). Subsequently, high EGFR level in the GSCs was used as a marker for isolating the GSCs from the EC (**Figure S3A**). The EC population isolated from the BBB organoids (EC_{BBB}), and GSC monocultures ($Mono_{184}$ and $Mono_{401}$) were used as controls.

Figure S3B shows a principal component analysis (PCA) plot depicting significant separation in the distribution of genetic variation between GSCs isolated from the BTB organoids (GSC_{BTB}) and their respective monoculture groups (GSC_{Mono}), as well as between the EC_{BTB} and EC_{BBB} population, suggesting that this specific co-culture approach have a major effect on the genomic alterations of these cells. Differential expression gene (DEG) analysis was performed to compare the transcriptomic changes between each GSC_{BTB} and their respective GSC_{Mono}. GSC from BTB_{184} had 1166 upregulated genes and 661 downregulated genes (**Figure 3A**), while GSC from BTB_{401} displayed 589 upregulated genes and 44 downregulated genes (**Figure 3B**).

Commonly enriched pathways amongst the upregulated genes in both the GSC models include cytokine-cytokine receptor interaction, ECM-receptor interaction, protein digestion and absorption, focal adhesion, PI3K-AKT and MAPK signaling pathways (**Figure 3C and 3D**). Many of these pathways are critical for cytoskeletal reorganization and cell locomotion, which are important for promoting GBM cell adhesion, proliferation, motility and apoptosis resistance[45,46]. GSC from each BTB_{184} (primary) and BTB_{401} (recurrent, from the same patient) also displayed several distinctively enriched pathways. For example, inflammatory-related pathways such as TNF, NF-κB, and IL-17 signaling pathways known to promote tumor invasion[47]

were enriched in the GSC of BTB_{184} (**Figure 3C**), while GSC from BTB_{401} showed enrichment in EGFR tyrosine kinase inhibitor resistance, calcium signaling pathway, vascular smooth muscle contraction that are involved in tumor progression, angiogenesis and resistance to drugs[48,49] (**Figure 3D)**. Hallmark pathway analysis of the upregulated genes revealed the enrichment of mTORC1 signaling, hypoxia, glycolysis, and E2F targets pathways in the GSC of BTB_{401} compared to BTB_{184} (**Figure S3D**), suggesting that the recurrent cells are more proliferative, pro-angiogenic, and resistant to therapy relative to the primary cells.

We identified 142 overlapping genes (GSC_{common}) that were upregulated in both GSC_{BTB} groups compared to their respective GSC_{Mono} (**Figure 3E)**. Gene Ontology (GO) analysis of these overlapping genes showed several enriched biological processes, including those related to ECM organization, extracellular structure organization, angiogenesis, and blood vessel morphogenesis (**Figure 3F**). Epithelial-mesenchymal transition (EMT) was identified to be the most enriched hallmark amongst the overlapped genes (**Figure S3C**). Correspondingly, TNF-α/NF-κB signaling that is crucial for inducing EMT in invading tumor cells were also highly upregulated[50,51]. Further GO analysis revealed downregulated genes related to processes such as nervous system development, neurogenesis and cell differentiation (**Figure S3E**). Based on GSC categorization that was previously established, constructive GSCs are enriched for developmental pathways related to neuron, brain and glial cells, while invasive GSCs are driven by enrichment of ECM and angiogenesis pathways[52]. These findings point to the critical role of NVU cells in reprogramming the GSCs to adopt a more invasive state over the constructive state.

GSC_{BTB} exhibit enhanced features seen in clinical GBM samples

Next, we assessed the expression of key regulatory genes obtained from two publicly available GBM patient datasets (GSE145645 and GSE147252) from the Gene Expression Omnibus (GEO) repository. Differential expression analysis was used to verify that these genes are prevalent in majority of GBM patient samples compared to low-grade glioma and normal brain tissue (**Figure S3F and S3G**). We observed significant upregulation of several of these prominent genes in GSC_{BTB} compared to GSC_{Mono} (**Figure 3G)** that are typically enriched in GBM patient samples, particularly related to stemness, EMT, invasion/migration, angiogenesis, hypoxia, inflammatory response, and ECM remodeling[53–55].

Hallmark genes related to stemness, EMT and invasion were upregulated in GSC_{BTB}, indicating that co-culture with NVU cells activate the GSCs to adopt a mesenchymal phenotype with greater invasive and self-renewal characteristics. Furthermore, extensive ECM remodeling in GSC_{BTB} characterized by the upregulation of ECM-associated genes is observed (**Figure 3G**). The ECM of GBM is associated with overexpression of components such as fibronectin, tenascin-C, and hyaluronan[56,57] and extensive deposition of fibrillar collagen compared to normal brain[58]. Upregulation of ECM related genes such as FN1, TNC, CD44 and COL4A1 was found in GSC_{BTB} relative to GSC_{Mono}, consistent with the expected aberrant ECM composition of GBM that serves to promote tumor growth, invasion and angiogenesis[59].

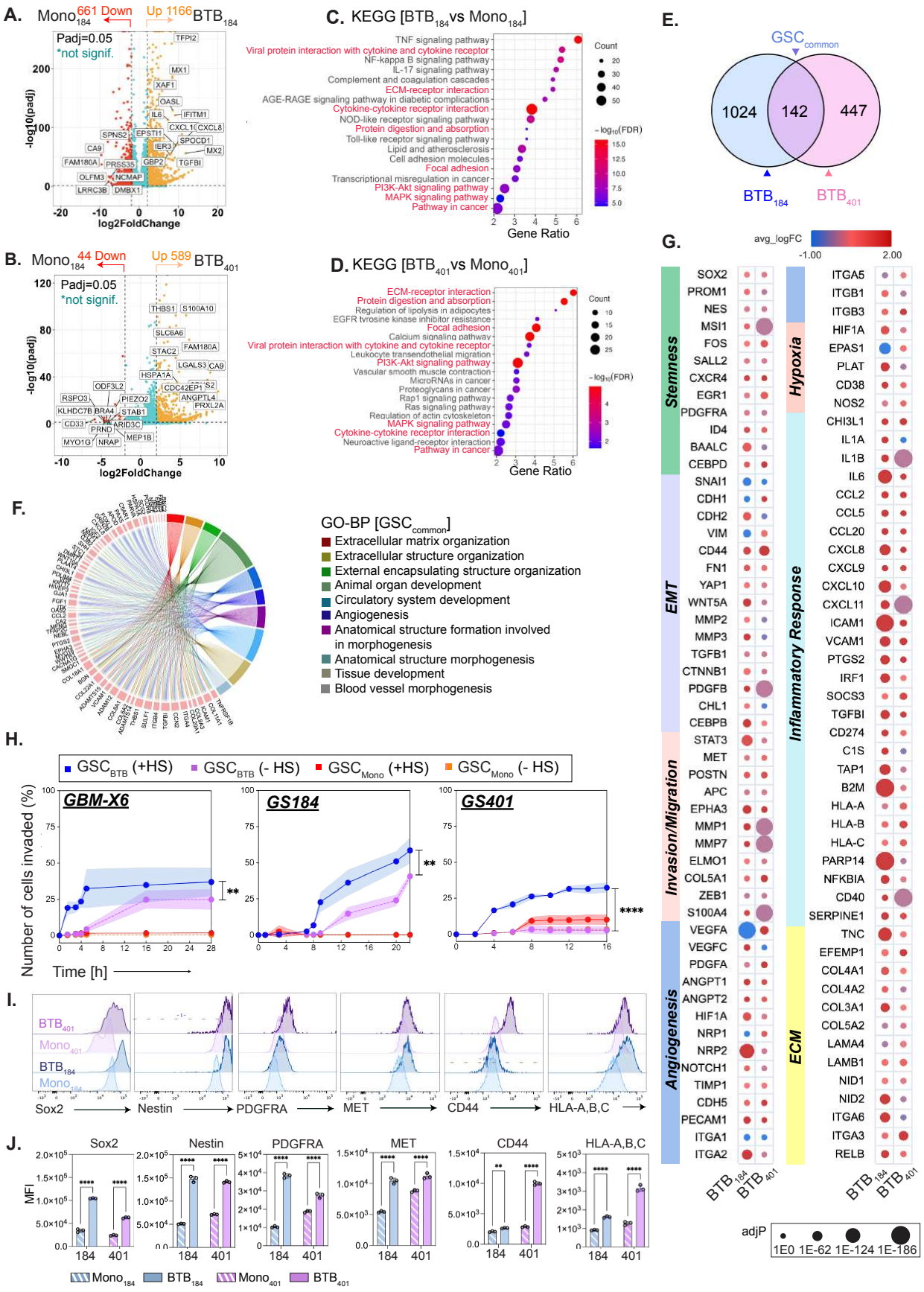
A.
Mono184 661 Down Up 1166 BTB184
Padj=0.05
*not signif.
-log10(padj)
log2FoldChange
B.
Mono184 44 Down Up 589 BTB401
Padj=0.05
*not signif.
-log10(padj)
log2FoldChange
C. KEGG [BTB184 vs Mono184]
TNF signaling pathway
Viral protein interaction with cytokine and cytokine receptor
NF-kappa B signaling pathway
IL-17 signaling pathway
Complement and coagulation cascades
ECM-receptor interaction
AGE-RAGE signaling pathway in diabetic complications
Cytokine-cytokine receptor interaction
NOD-like receptor signaling pathway
Protein digestion and absorption
Toll-like receptor signaling pathway
Lipid and atherosclerosis
Cell adhesion molecules
Focal adhesion
Transcriptional misregulation in cancer
PI3K-Akt signaling pathway
MAPK signaling pathway
Pathway in cancer
Count
-log10(FDR)
Gene Ratio
D. KEGG [BTB401 vs Mono401]
ECM-receptor interaction
Protein digestion and absorption
Regulation of lipolysis in adipocytes
EGFR tyrosine kinase inhibitor resistance
Focal adhesion
Calcium signaling pathway
Viral protein interaction with cytokine and cytokine receptor
Leukocyte transendothelial migration
PI3K-Akt signaling pathway
Vascular smooth muscle contraction
MicroRNAs in cancer
Proteoglycans in cancer
Rap1 signaling pathway
Ras signaling pathway
Regulation of actin cytoskeleton
MAPK signaling pathway
Cytokine-cytokine receptor interaction
Neuroactive ligand-receptor interaction
Pathway in cancer
Count
-log10(FDR)
Gene Ratio
E.
GSCcommon
1024
142
447
BTB184
BTB401
G.
avg_logFC
-1.00
2.00
Stemness
SOX2
PROM1
NES
MSI1
FOS
SALL2
CXCR4
EGR1
PDGFRA
ID4
BAALC
CEBPD
EMT
SNAI1
CDH1
CDH2
VIM
CD44
FN1
YAP1
WNT5A
MMP2
MMP3
TGFB1
CTNNB1
PDGFB
CHL1
CEBPB
Invasion/Migration
STAT3
MET
POSTN
APC
EPHA3
MMP1
MMP7
ELMO1
COL5A1
ZEB1
S100A4
Angiogenesis
VEGFA
VEGFC
PDGFA
ANGPT1
ANGPT2
HIF1A
NRP1
NRP2
NOTCH1
TIMP1
CDH5
PECAM1
ITGA1
ITGA2
Hypoxia
ITGA5
ITGB1
ITGB3
HIF1A
EPAS1
PLAT
CD38
NOS2
Inflammatory Response
CHI3L1
IL1A
IL1B
IL6
CCL2
CCL5
CCL20
CXCL8
CXCL9
CXCL10
CXCL11
ICAM1
VCAM1
PTGS2
IRF1
SOCS3
TGFBI
CD274
C1S
TAP1
B2M
HLA-A
HLA-B
HLA-C
PARP14
NFKBIA
CD40
SERPINE1
ECM
TNC
EFEMP1
COL4A1
COL4A2
COL3A1
COL5A2
LAMA4
LAMB1
NID1
NID2
ITGA6
ITGA3
RELB
BTB184
BTB401
adjP
1E0
1E-62
1E-124
1E-186
F.
GO-BP [GSCcommon]
Extracellular matrix organization
Extracellular structure organization
External encapsulating structure organization
Animal organ development
Circulatory system development
Angiogenesis
Anatomical structure formation involved in morphogenesis
Anatomical structure morphogenesis
Tissue development
Blood vessel morphogenesis
H.
GSCBTB (+HS)
GSCBTB (- HS)
GSCMono (+HS)
GSCMono (- HS)
GBM-X6
GS184
GS401
Number of cells invaded (%)
Time [h]
I.
BTB401
Mono401
BTB184
Mono184
Sox2
Nestin
PDGFRA
MET
CD44
HLA-A,B,C
J.
Sox2
Nestin
PDGFRA
MET
CD44
HLA-A,B,C
MFI
184
401
Mono184
BTB184
Mono401
BTB401

Figure 3. **Genomic profiling of GSCs shows enhanced tumor aggressiveness in BTB organoids.**
(A, B) Volcano plot showing differential expression of genes between **(A)** BTB_{184} and $Mono_{184}$; **(B)** BTB_{401} and $Mono_{401}$. (log2 fold change > 2, padj < 0.05).
(C, D) KEGG analysis of the upregulated genes displaying the enriched pathways in **(C)** BTB_{184} and **(D)** BTB_{401}. (False discovery rate (FDR) < 0.05). Commonly enriched pathways in both BTB_{184} and BTB_{401} are highlighted in red.
(E) Venn diagram identified 142 overlapping genes (GSC_{common}) that is upregulated in both the BTB_{184} and BTB_{401} groups.
(F) Gene ontology chord plot showing the top 10 enriched biological processes (BP) for GSC_{common} and the genes involved in each BP.
(G) Bubble heatmap displaying gene expression fold change (FC) in the GSCs of BTB_{184} and BTB_{401} organoids compared to the respective controls, $Mono_{184}$ and $Mono_{401}$. Genes associated with stemness, epithelial-mesenchymal transition (EMT), invasion/migration, angiogenesis, hypoxia, inflammatory response, and extracellular matrix (ECM) remodeling were compiled from literatures[60,61].
(H) Measurement of cell invasion using the transwell invasion assay (refer to **Figure S3H**) comparing between the GSC_{BTB} and GSC_{Mono} groups. GSC invasion is tracked using time-lapse imaging. Quantification of the total number of GSCs that have invaded to the basal side of the transwell insert shows that GSC_{BTB} are more invasiveness than GSC_{Mono}. (Data are represented as mean ± s.d. One-way ANOVA with Dunnett's multiple comparisons test, n=3 in each group, **P < 0.01, ****P < 0.0001).
(I) Flow cytometry analyses of protein expression of the representative genes related to stemness, EMT, invasion and inflammation (SOX2, Nestin, MET, CD44, PDGFRA, HLA-A, B, C) in GSC_{BTB} and GSC_{Mono}.
(J) Quantification of mean fluorescence **(from I)** demonstrates enhanced mesenchymal and self-renewal features in GSC_{BTB} compared to GSC_{Mono}. (n=3, two-way ANOVA and Sidak's multiple comparison test, data are represented as mean ± s.d., **P < 0.01, ****P < 0.0001).

To further verify the invasiveness of GSC_{BTB} compared to GSC_{Mono}, dissociated GSCs were inserted onto the apical side of a transwell coated with Matrigel, and the GSCs were allowed to invade into the bottom basolateral side of the transwell using human serum as a chemoattractant (**Figure S3H**). A significantly higher proportion of GSC_{BTB} invaded into the bottom of the transwells compared to GSC_{Mono} (**Figure 3H).** Flow cytometry analysis demonstrated increased expression of several markers known to promote GBM aggressiveness, including *SOX2, NESTIN*, *PDGFRA*, *MET*, *CD44*, and *HLA-A, B, C* in the GSC_{BTB} compared to GSC_{Mono} (**Figure 3I and 3J)**.

Genomic alterations in EC_{BTB} bolster tumor progression

The dynamic interaction between GBM cells and the brain microvascular alters tissue homeostasis to foster tumor progression[1]. DEG analysis of the EC population revealed 203 and 183 upregulated genes in BTB organoids established with GS184 and GS401 (EC_{184} and EC_{401}), respectively compared to EC isolated from control BBB organoids (EC_{BBB}) (**Figure S4A**). While only ~8% of upregulated genes in GSC_{common} overlapped (**Figure 3E**) signifying notable inter-heterogeneity, ~64% of the upregulated genes overlapped between EC_{184} and EC_{401} (EC_{common}) (**Figure S4C)**, indicating relatively homogeneous activation of similar pathways in the disruption of vascular processes by the GSCs.

Kyoto Encyclopedia of Genes and Genomes (KEGG) pathway analysis of the EC_{common} genes identified the enrichment of inflammation-related pathways including IL-17, TNF and NF-κB signaling pathways[63] (**Figure S4D**), pointing toward BBB disruption and injury response processes in the presence of GBM cells. Hallmark pathway analysis also revealed the enrichment of EMT and angiogenesis pathways in EC_{common}

(**Figure S4B**). Indeed, evidence has shown that the inflammatory GBM microenvironment induces EMT in a subset of the EC population[64], which can contribute to resistance to anti-angiogenic therapy[65], chemoresistance[66] and radio-resistance[67]. Hypoxic pathways were also enriched in EC_{common}, aligning with the promotion of angiogenesis (**Figure S4B**).

KEGG and gene ontology (GO) analyses revealed several downregulated genes (EC_{down}) in the BTB organoids related to processes such as axon guidance, neurogenesis, nervous system development and differentiation (**Figure S4E**). Indeed, BBB perturbation are known to lead to neuronal dysfunction, neuroinflammation and neurodenegeneration[62,68]. A prior study has identified a set of 78 upregulated genes associated with malignant GBM vasculatures in patients compared to normal brain vessels[69]. Out of the 78 genes, 46 (in EC_{184}) and 40 (in EC_{401}) genes were upregulated compared to the control EC_{BBB} (**Figure S4F**). This is a major improvement in comparison to a recent report[34], which identified only 24 upregulated genes (out of the 78) in ECs isolated from primary and secondary human GBM compared to control vessels.

GSCs from BTB organoids are more aggressive than the monocultures *in vivo*

Orthotopic GBM xenografts were established in mice through intracranial injection of dissociated single cells from the BTB_{184}, $Mono_{184}$ or BBB (control) organoid group, as depicted in **Figure S5A**. For the monoculture group, dissociated GS184 cells were mixed with each NVU monoculture cells in the same ratio as the organoid coculture group immediately before tumor implantation. GBM tumors were established intracranially in the right frontal lobe and allowed to grow for 8-10 weeks. *Ex vivo* analysis of brain cryosections at 8 weeks showed engraftment of the GS184 cells in both the BTB_{184} and $Mono_{184}$ groups, as identified through immunohistochemistry staining of human vimentin (**Figure 4A)**. Evidenced by flow cytometry and immunofluorescence staining, NVU cells also express abundant human vimentin (**Figure S5B**). Therefore, as a control, dissociated cells from BBB organoids were established intracranially in the same manner. No vimentin signal was detected throughout the brain section (**Figure S5C**), indicating that the NVU cells did not survive/propagate in the mouse brain, and that human vimentin thus served as an effective marker for visualizing the GSC population.

After 8 weeks, a significant level of GSC from the BTB_{184} group had migrated along the corpus callosum (CC) and invaded into the cortex (CX), whereas the tumor from the $Mono_{184}$ group appeared compact with significantly fewer cells in the CC and CX (**Figure 4A, S5C**). At 10 weeks post-implantation, compared to the $Mono_{184}$ group, GSC from the BTB_{184} group showed significantly higher level of growth spread throughout the right hemisphere and invasion along the white matter tracts including the CC and anterior commissure (AC), reaching the CX and contralateral left hemisphere (**Figure 4B**). Quantification of tumor coverage using several brain sections showed that GSC from BTB_{184} occupied a larger area in the brain compared to tumor cells from the $Mono_{184}$ group (**Figure 4C)**, further substantiating that the GSC from the BTB_{184} group are more infiltrative.

Next, we evaluated astrocytic activation by immunofluorescence staining for GFAP[70]. Astrocytes, comprising 40-50% of brain cells, are known to be activated by glioma cells, adopting a reactive phenotype[71,72]. Reactive astrocytes, characterized by hypertrophy and increased GFAP expression, directly associate with GBM cells to aid tumor progression, mesenchymal transition and therapeutic resistance[25,70,73]. In both the BTB_{184} and $Mono_{184}$ groups, we observed a high level of GFAP-positive reactive astrocytes in the peritumoral region, with significantly higher GFAP expression in the BTB_{184} group (**Figure 4A and**

S5C). This observation corresponds with our earlier results showing the tendency of astrocytes to congregate in proximity to the GSCs within the BTB organoids (**Figure 1D**).

Concurrent activation of astrocytes and microglia have been recognized for their pivotal role in promoting GBM malignancy and invasiveness[74]. Early histological analyses have also documented that GBM-associated macrophages and microglia (GAMs) are more enriched in mesenchymal GBM[75,76]. Immunostaining for IBA1 showed significantly higher level of activated microglia clustering around the tumor in the BTB_{184} group compared to the $Mono_{184}$ group (**Figure 4A, S5C**), further implicating the GSC from the BTB_{184} group in having more invasive and mesenchymal features.

GSC from BTB organoids exacerbate BBB leakage and neovascularization

We further examined GBM-induced alteration of the blood vessels in brain regions where there was either a 'dense' or 'sparse' population of tumor cells (**Figure 4D**). Immunofluorescence staining for CD31 revealed that in both the BTB_{184} and $Mono_{184}$ groups, regions with a high density of tumor cells exhibited more disorganized and tortuous blood vessels, as well as an increased in microvascular density (MVD), relative to areas with sparse tumor population (in the contralateral hemisphere) and the control group (healthy brain) (**Figure 4D, 4E**). Intravenous administration of TRITC-dextran was used to assess vessel permeability. We observed increased dextran accumulation in the brain parenchyma indicating enhanced vessel permeability and compromised BBB integrity within the BTB_{184} group compared to the $Mono_{184}$ group, especially within the tumor-dense areas (**Figure 4F, 4G).** In healthy brain tissues and regions with sparse tumor population, the dextran signal remained confined within the blood vessels, suggesting the maintenance of intact BBB integrity (**Figure 4D, 4F**).

A significant subpopulation of tumor cells from the BTB_{184} group expressed the endothelial markers CD31 and CD105 (**Figure 4H, 4I**), suggesting these GSC had undergone endothelial transdifferentiation to acquire endothelial-like properties[77]. This process is known to be important for supporting tumor growth and enhance tumor invasiveness and resilience against anti-angiogenic therapies[78].

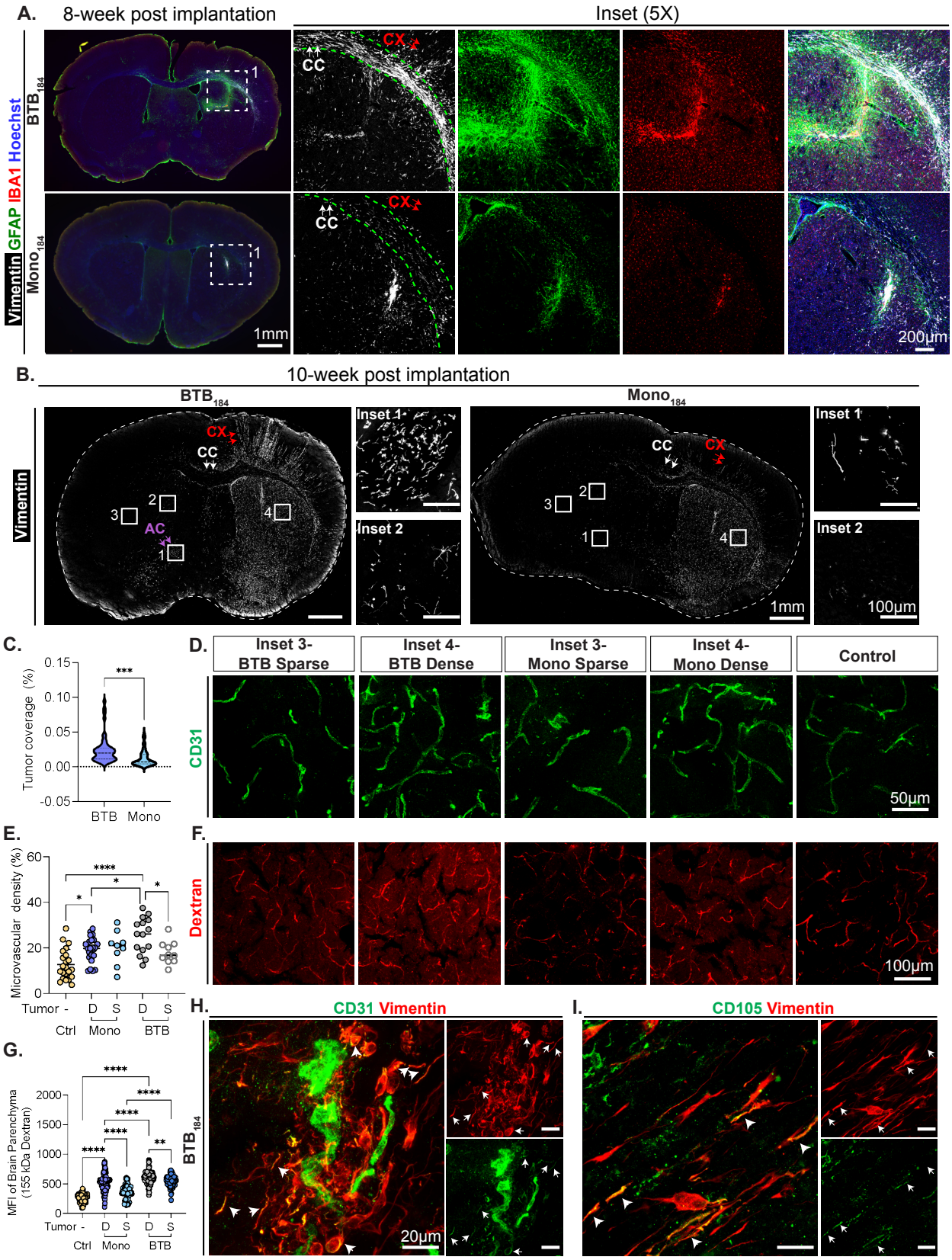

Figure 4. GSC from BTB organoids are more aggressive than the monoculture in orthotopic PDX mouse models.

(A) Immunofluorescence staining of coronal brain cryosections showing engraftment of GSC from BTB_{184} and $Mono_{184}$ in mice at 8 weeks. Whole brain sections are stained with Vimentin, GFAP and IBA1 to visualize the GSC, astrocytes, and GBM associated macrophages and microglia (GAM), respectively. Insets (5X) showing the magnified areas specified in the whole brain slices (left). CC: corpus callosum (white arrows), CX: cortex (red arrows). Green dash line outlines the CC region. Scale bar, whole brain sections: 1mm; inset: 200 µm.
(B) Invasion of GSC from BTB_{184} and $Mono_{184}$ at 10 weeks post-implantation in mice brain. AC: anterior commissure (purple arrows). Insets 1 and 2 show the magnified views of selected regions in the contralateral hemisphere of the brain section. GSC from BTB_{184} exhibits higher invasion through the white matter tracts CC and AC, and into the cortex and contralateral hemisphere.
(C) Graph showing the percentage of GSC coverage in BTB_{184} and $Mono_{184}$ in mice brain. Results are quantified from 15-20 serial coronal cryosections per mouse (n=3-4 mice each group, unpaired t test with Welch's correction, ***P < 0.001).
(D) Representative fluorescence images and quantification **(E)** of microvascular density (CD31 staining) in the BTB_{184} and $Mono_{184}$ groups. Images showing magnified view of insets 3 and 4 outlined from panel **(B)** represent tumor-sparse and tumor-dense regions in the BTB_{184} and $Mono_{184}$ groups, respectively. Scale bar, 50 µm. (n = 3-4, one-way ANOVA with Tukey's multiple comparisons test, *P < 0.1, ****P < 0.0001).
(F) Representative confocal images and quantification **(G)** showing the perivascular signal of TRITC dextran in the BTB_{184} and $Mono_{184}$ groups. No significant change in dextran permeability is observed in the tumor-sparse areas compared with the control (healthy brain with no tumor). A significant increase in dextran signal outside the vessels is detected in the tumor-dense regions, with the highest leakage observed in the BTB_{184} group. Scale bars, 100 µm. (n = 3-4, one-way ANOVA with Tukey's multiple comparisons test, ****P < 0.0001, **P < 0.01).
(H, I) Representative images showing endothelial transdifferentiation in the BTB_{184} group. Immunofluorescence staining of brain cryosections for the tumor cells with human vimentin (red) with CD31 and CD105 (green). Arrows (white) indicate colocalization of vimentin with CD31**(H)** and CD105 **(I)**. Scale bars, 20 µm.

Modeling therapeutics delivery and efficacy

GBM targeting using BTP-7 peptide

As a proof-of-concept to validate the BTB organoids as a therapeutic testing platform, we employed a known GBM-targeting peptide, known as the deglycosylated Brevican (dg-Bcan)-Targeting Peptide-7 (BTP-7)[18]. Brevican (Bcan), an ECM glycoprotein presents a unique de-glycosylated isoform dg-Bcan that is found only in human high-grade gliomas[18,79], and is absent in healthy CNS and other non-cancerous neuropathological tissues. Previous studies have established that BTP-7 *i)* binds dg-Bcan recombinant protein specifically**,** *ii)* targets GBM tumors in patient-derived xenograft (PDX) mouse models, *iii)* is specifically taken up by GSCs compared to other NVU cells, and *iv)* crosses the BBB in both human organoids and in mice[16,18].

Western blot analysis confirmed dg-Bcan expression in all of our patient-derived GSC models (**Figure S6A**). Incubation of Cy5-labeled BTP-7 with the BTB organoids, followed by a period of washout showed BTP-7 was preferentially retained in the GSCs, while displaying greater clearance rate in the NVU cells in both the BTB and BBB organoids (**Figure 5A, 5B, S6B**). These results align with our previous *in vivo* observation which demonstrated effective targeted delivery of BTP-7 to GBM tumors in orthotopic PDX mouse models[16,18].

Gene therapy using Adeno-Associated Viruses (AAVs)-AAV.CPP.16

We further investigated the BTB organoid model for predicting therapeutic outcome using the adeno-associated viruses functionalized with a cell-penetrating peptide (AAV.CPP.16), where its ability to cross the BBB and efficacy for GBM treatment *in vivo* has been previously established[14]. First, AAV.CPP.16 transcytosis/permeability was confirmed in both the BBB and BTB organoids by confocal microscopy, where AAV-transduced cells at >50 μm depth was observed in all organoids. (**Figure S6D**).

To investigate GBM-targeting, we assessed the delivery of AAV.CPP.16-GFAP, which harbors a GFAP promoter to transduce only GFAP-positive cells. Western blot analysis shows that GFAP is expressed most abundantly in GS401 followed by GBM-X6 cells compared to astrocytes (**Figure S6C**). We observed significant level of AAV colocalization with the GSCs in the BTB organoids across all the groups (**Figure 5C, 5D, 5E**). A box plot representing the mean intensity within a specified region of interest in the BTB organoids (selected based on tumor density) depicts significant overlap between the AAV and GSC signal (**Figure 5D, 5E**), confirming efficient transduction and selectivity of AAV.CPP.16-GFAP for the GSC.

Next, we measured the therapeutic efficacy of AAV.CPP.16-GFAP in delivering the Herpes simplex virus type 1 thymidine kinase (HSV-TK1), a suicide gene that metabolizes the prodrug ganciclovir (GCV) into a cytotoxic compound[14]. Upon formation, the organoids were treated with AAV.CPP.16-GFAP-TK1 (Figure 6F), and then administered with 8 μM of GCV (for 8 h, followed by 16 h incubation in fresh medium) daily for over a 9-day period (**Figure 5F**). The GCV concentration was optimized based on our study showing that concentrations of 8 μM or less does not affect the permeability of intact BBB organoids to dextran (**Figure S6E**). Confocal microscopy revealed a marked reduction in tumor volume in the AAV-treated groups, while GSC growth and infiltration continued to progress in the control groups that did not receive the combinatorial AAV and GCV treatment (**Figure 5G, S6F, S6G**). To quantify the treatment response, the BTB organoids were dissociated into single cells on specific days during the treatment course, and the number of GSC relative to Day 0 was measured. In the control groups, significant tumor progression is observed (1.8-, 3.9-, and 2.4-fold increase in tumor cell count for GBM-X6, GS184 and GS401, respectively by Day 9). In contrast, a significant decline in tumor cell number (95-99% by Day 9 relative to Day 0) is observed in the AAV-treated groups. This result is consistent with the previous findings *in vivo*[14], where AAV.CPP.16-GFAP-TK1 and GCV therapy in tumor-bearing mice led to substantial tumor volume shrink. This highlights the potential of the BTB organoids as a rapid and predictive pre-clinical screening tool for GBM therapeutics.

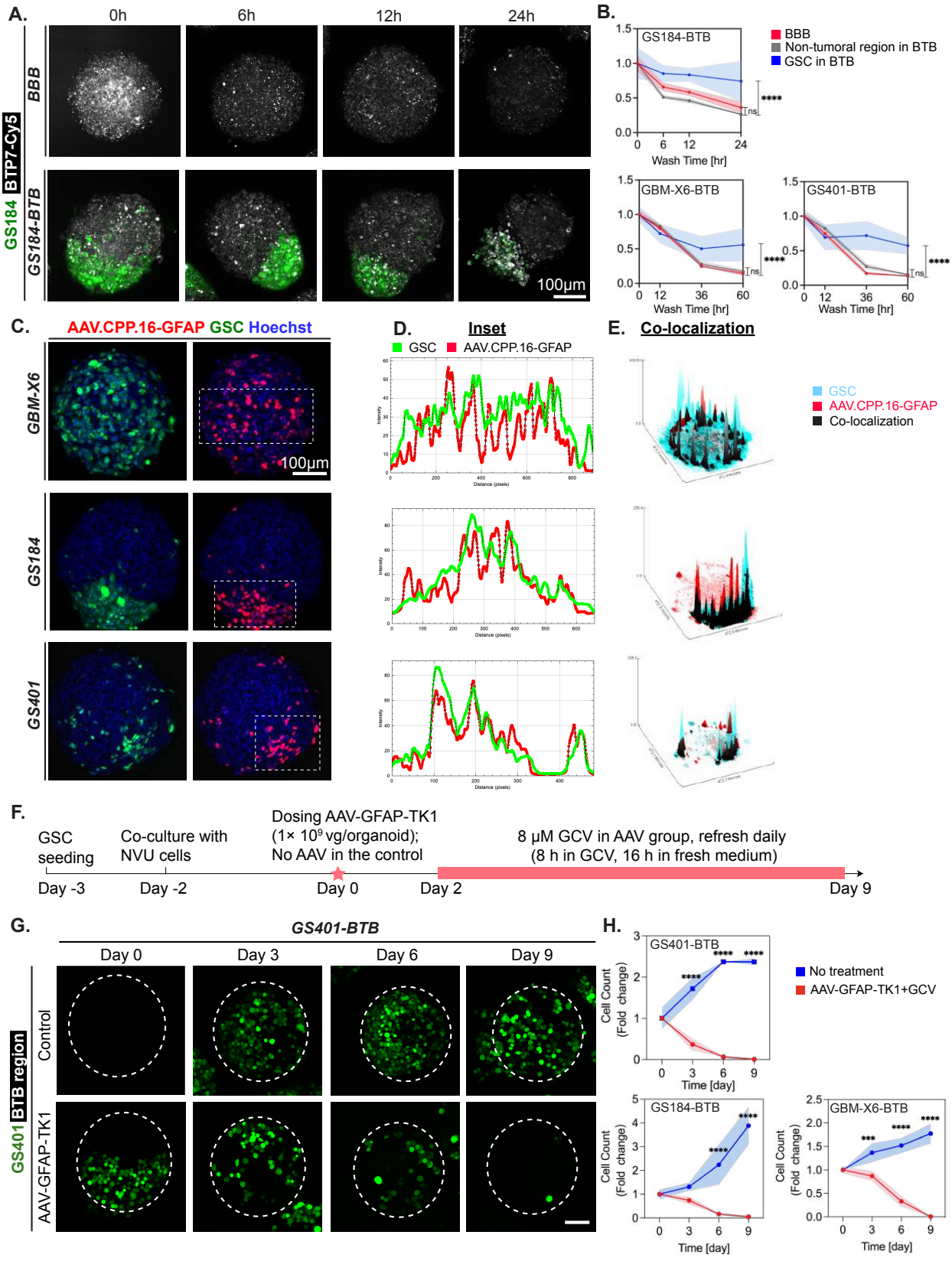

Figure 5. Modeling therapeutics delivery and efficacy using BTB organoids.

(A, B) Representative fluorescence images **(A)** and quantification of mean fluorescence intensity **(B)** displaying the distribution of BTP-7-Cy5 (white) in BBB and BTB organoids over a washout period (refer also to **Figure S6B**). After 4h-incubation with BTP-7-Cy5, the organoids are washed for a period starting at 0 h (up to 60 h). BTP-7-Cy5 is specifically retained in the GSCs over time, while displaying greater clearance rate in the NVU cells. (n = 6-8, two-way ANOVA with Dunnett's multiple comparison test, mean ± s.d., ****P < 0.0001, ***P < 0.001, **P < 0.01, *P < 0.05).

(C) Representative confocal images showing AAV-labeled cells in GBM-X6-, GS184- and GS401-BTB organoids after incubating with 1×10^9 vg of AAV.CPP.16-GFAP (red) for 72 h. Scale bar, 100 □m.

(D) Average intensity profile depicting the of GSCs (green) and AAV.CPP.16-GFAP (red) in the ROI (depicted by white dash box in **(C)**).

(E) 3D plot showing the co-localization (black) between the GSC (cyan) and the AAV.CPP.16-GFAP (red).

(F) Timeline of AAV.CPP.16-GFAP-TK1 therapy combined with Ganciclovir (GCV) in GS401-BTB organoids. Organoids are treated with AAV (1×10^9 vg/organoid), followed by addition of 8 □M GCV after 48 h until day 9, with GCV refreshed every day. BTB organoids were incubated with GCV for 8h and 16h in fresh medium.

(G) Representative confocal images of the treated and non-treated GS401-BTB organoids over the 9-day treatment period.

(H) Quantification plot (n=4) showing the GSC count fold change in the treated and non-treatment groups. Data are represented as mean ± s.d., two-way ANOVA with Sidak's multiple comparison test, ****P < 0.0001, ***P < 0.001, **P < 0.01.

Discussion

Malignant brain tumors are particularly difficult to treat compared to other cancers, and a major factor is attributed to the presence of the BBB. Conventional experimental GBM models utilizing patient-derived GSC cultured as tumor spheres have been vital in advancing brain tumor research and the development of new treatments. However, GSC monocultures do not capture the complex cellular interactions with NVU cells that is known to have significant implications in tumor progression, aggressiveness and angiogenesis. Although GSC monocultures are typically maintained in serum free condition, the BTB organoids are cultured in the presence of a low concentration of human serum. It is possible that the presence of serum and NVU cells may contribute towards mimicking the landscape of the tumor microenvironment in a living brain. Collectively, our transcriptomic analyses reveal substantial alternations in the genomic profile of the tumor cell population when cultured in the form of the BTB organoid compared with their corresponding monocultures. The identified pathways are largely involved in the promotion of EMT, stemness, invasion, ECM remodeling and neovascularization, and this is further supported by our cell invasion assays, *in vivo* results, as well as the genomic features that have previously been identified in GBM patient tissues.

In a corresponding manner, the endothelial population in the BTB organoids also displays significant transcriptomic changes compared to EC attained from BBB organoids without tumor cells, including upregulation of pathways involved in angiogenesis, inflammatory response, EMT and hypoxia, which are hallmarks of GBM[80]. Several upregulated ligand-receptor pairs between the tumor and endothelial populations have been identified here, highlighting the significant level of crosstalk that occurs when the cells are co-cultured in the organoid. Indeed, we found that the tumor condition media alone in the absence of direct GBM-EC contact had little to no impact on the permeability of BBB organoids (**Figure 2B**). For BTB studies and therapeutic testing, the transwell system remains the most widely utilized *in vitro* model[5], where the EC and tumor population are often cultured in separate compartments, allowing each cell type to

be mostly influenced by only the condition media. With growing evidence to support the crucial role of direct cell-cell interaction for modeling brain tumors and the BTB, the implementation of direct co-cultures in experimental models ought to be considered.

NVU cells in the tumor niche, such as pericytes and astrocytes are also known to directly communicate with GBM cells. GBM-pericyte crosstalk activates processes such as vascular cooption and mimicry, as well as alters pericyte transcriptome to facilitate tumor evasion of immune response[81]. Astrocyte-GBM interactions have been implicated in changes in ECM components, chemokines, cytokines and cytoskeletal rearrangements to promote tumor progression[74]. Although the roles of pericytes and astrocytes in our BTB organoids have yet to be thoroughly examined, it is likely that these cell populations also significantly contribute to the various gene, protein and functional alterations of the GSC in the BTB organoid. Indeed, we observe that astrocytes tend to reorganize themselves in spatial proximity to the tumor cells in the BTB organoids (**Figure 1D**), a phenomenon that has also been reported *in vivo*[70,71] and play important functions in EMT, tumor invasiveness and therapeutic resistance[26]. Collectively, the BTB organoid model offers a dynamic *in vitro* system that allows for studying the plasticity of the tumor microenvironment and the influence of various complex intercellular communications on the disease progression.

GSCs in the BTB organoids exhibit downregulated pathways related to neuronal development. In the future, other cell types of the NVU within the tumor microenvironment, such as neurons and immune cells can be incorporated into the organoids to further advance the model. This platform can also be adapted to utilize iPSCs to establish personalized and translational therapeutic strategies in the long term. Future work can also focus on using single-cell RNA sequencing to characterize intratumoral GSC heterogeneity within the BTB organoids.

Even though the BTB organoid system lacks the integration of laminar flow to simulate blood flow, it has proven success for modeling therapeutic targeting and drug response, though more studies using various established and investigational drugs in the future will further validate this model. While conventional GSC models alone have been valuable for measuring the cytotoxic effects on tumor cells, the BTB organoids offer the additional benefit of enabling the evaluation of drug delivery across the BTB, off-target effects on the normal NVU cell types, as well as the influence of the drug on BBB/BTB function. Information from these studies can be rapidly attained and aid investigators in prioritizing the most promising compounds for further evaluation *in vivo*. Jacob *et. al.* have previously described a clinically relevant patient-derived GBM organoid (GBO) model that is established using freshly resected GBM tissues formed over 2 weeks[7]. Our BTB organoids feature many similar strengths presented by the GBO model, including resemblance to histological phenotypes, cellular diversity, and genetic expression typically seen in GBM patient tissues, as well as proficiency in modeling therapeutic delivery. The BTB organoid platform presents more versatility than the GBO model in terms of compatibility with using other brain tumor cell cultures, and so do not necessarily rely on the procurement of freshly resected tumor tissues if they are not available, as they may be difficult to attain in many laboratories. The organoids can be formed rapidly within 3 days (instead of weeks) to further expediate therapeutic assessment.

The BTB organoid platform is scalable to high-throughput capacity, cost effective, straightforward to use, and highly accessible to most laboratories. For therapeutic detection and analysis, confocal microscopy or mass spectrometry approaches can be implemented[12], and screening throughput can be further increased through integration with automated microscopes and robotics-assisted mass spectrometry technologies. All

in all, the BTB organoid platform is a highly relevant model that faithfully recapitulates various important features of the BTB observed in the clinic and *in vivo*, and can offer a practical approach for expediting drug screening and facilitating translational research in brain tumors.

References

1. Enam, S. F. *et al.* Cytostatic hypothermia and its impact on glioblastoma and survival. *Sci. Adv.* **8**, eabq4882 (2022).
2. Straehla, J. P. *et al.* A predictive microfluidic model of human glioblastoma to assess trafficking of blood–brain barrier-penetrant nanoparticles. *Proc. Natl. Acad. Sci.* **119**, e2118697119 (2022).
3. Janjua, T. I. *et al.* Frontiers in the treatment of glioblastoma: Past, present and emerging. *Adv. Drug Deliv. Rev.* **171**, 108–138 (2021).
4. Hajal, C., Le Roi, B., Kamm, R. D. & Maoz, B. M. Biology and Models of the Blood-Brain Barrier. *Annu. Rev. Biomed. Eng.* **23**, 359–384 (2021).
5. Prashanth, A. *et al.* Are In Vitro Human Blood–Brain–Tumor-Barriers Suitable Replacements for In Vivo Models of Brain Permeability for Novel Therapeutics? *Cancers* **13**, 955 (2021).
6. Steeg, P. S. The blood–tumour barrier in cancer biology and therapy. *Nat. Rev. Clin. Oncol.* (2021) doi:10.1038/s41571-021-00529-6.
7. Jacob, F. *et al.* A Patient-Derived Glioblastoma Organoid Model and Biobank Recapitulates Inter- and Intra-tumoral Heterogeneity. *Cell* **180**, 188-204.e22 (2020).
8. Lee, J. *et al.* Tumor stem cells derived from glioblastomas cultured in bFGF and EGF more closely mirror the phenotype and genotype of primary tumors than do serum-cultured cell lines. *Cancer Cell* **9**, 391–403 (2006).
9. Sherman, H. & Rossi, A. E. A Novel Three-Dimensional Glioma Blood-Brain Barrier Model for High-Throughput Testing of Tumoricidal Capability. *Front. Oncol.* **9**, 351 (2019).

10. Deligne, C. *et al.* Development of a human in vitro blood–brain tumor barrier model of diffuse intrinsic pontine glioma to better understand the chemoresistance. *Fluids Barriers CNS* **17**, 37 (2020).
11. Xie, Z., Chen, M., Lian, J., Wang, H. & Ma, J. Glioblastoma-on-a-chip construction and therapeutic applications. *Front. Oncol.* **13**, (2023).
12. Cho, C.-F. *et al.* Blood-brain-barrier spheroids as an in vitro screening platform for brain-penetrating agents. *Nat. Commun.* **8**, 15623 (2017).
13. Bergmann, S. *et al.* Blood-brain-barrier organoids for investigating the permeability of CNS therapeutics. *Nat. Protoc.* **13**, 2827–2843 (2018).
14. Yao, Y. *et al.* Variants of the adeno-associated virus serotype 9 with enhanced penetration of the blood–brain barrier in rodents and primates. *Nat. Biomed. Eng.* (2022) doi:10.1038/s41551-022-00938-7.
15. Fadzen, C. M. *et al.* Perfluoroarene-Based Peptide Macrocycles to Enhance Penetration Across the Blood-Brain Barrier. *J. Am. Chem. Soc.* **139**, 15628–15631 (2017).
16. Cho, C.-F. *et al.* A Tumor-Homing Peptide Platform Enhances Drug Solubility, Improves Blood–Brain Barrier Permeability and Targets Glioblastoma. *Cancers* **14**, (2022).
17. Fadzen, C. M. *et al.* A Platinum(IV) Prodrug-Perfluoroaryl Macrocyclic Peptide Conjugate Enhances Platinum Uptake in the Brain. *J. Med. Chem.* **63**, 6741–6747 (2020).
18. von Spreckelsen, N. *et al.* Targeting Glioblastoma Using a Novel Peptide Specific to a Deglycosylated Isoform of Brevican. *Adv. Ther.* **4**, 2000244 (2021).

19. Lee, J. *et al.* Tumor stem cells derived from glioblastomas cultured in bFGF and EGF more closely mirror the phenotype and genotype of primary tumors than do serum-cultured cell lines. *Cancer Cell* **9**, 391–403 (2006).
20. Emlet, D. R. *et al.* Targeting a Glioblastoma Cancer Stem-Cell Population Defined by EGF Receptor Variant III. *Cancer Res.* **74**, 1238–1249 (2014).
21. Cho, C.-F. *et al.* Blood-brain-barrier spheroids as an in vitro screening platform for brain-penetrating agents. *Nat. Commun.* **8**, 15623 (2017).
22. Bergmann, S. *et al.* Blood-brain-barrier organoids for investigating the permeability of CNS therapeutics. *Nat. Protoc.* **13**, 2827–2843 (2018).
23. Liddelow, S. A. *et al.* Neurotoxic reactive astrocytes are induced by activated microglia. *Nature* **541**, 481–487 (2017).
24. Henrik Heiland, D. *et al.* Tumor-associated reactive astrocytes aid the evolution of immunosuppressive environment in glioblastoma. *Nat. Commun.* **10**, 2541 (2019).
25. Zhang, H., Zhou, Y., Cui, B., Liu, Z. & Shen, H. Novel insights into astrocyte-mediated signaling of proliferation, invasion and tumor immune microenvironment in glioblastoma. *Biomed. Pharmacother.* **126**, 110086 (2020).
26. Niklasson, M. *et al.* Mesenchymal transition and increased therapy resistance of glioblastoma cells is related to astrocyte reactivity. *J. Pathol.* **249**, 295–307 (2019).
27. Blethen, K. E. *et al.* Modulation of the blood-tumor barrier to enhance drug delivery and efficacy for brain metastases. *Neuro-Oncol. Adv.* **3**, v133–v143 (2021).
28. Sharma, A. & Shiras, A. Cancer stem cell-vascular endothelial cell interactions in glioblastoma. *Biochem. Biophys. Res. Commun.* **473**, 688–692 (2016).

29. Li, W., Chen, Z., Chin, I., Chen, Z. & Dai, H. The Role of VE-cadherin in Blood-brain Barrier Integrity Under Central Nervous System Pathological Conditions. *Curr. Neuropharmacol.* **16**, 1375–1384 (2018).
30. Andreone, B. J. *et al.* Blood-Brain Barrier Permeability Is Regulated by Lipid Transport-Dependent Suppression of Caveolae-Mediated Transcytosis. *Neuron* **94**, 581-594.e5 (2017).
31. Xie, Y. *et al.* Wnt signaling regulates MFSD2A-dependent drug delivery through endothelial transcytosis in glioma. *Neuro-Oncol.* **25**, 1073–1084 (2023).
32. Veys, K. *et al.* Role of the GLUT1 Glucose Transporter in Postnatal CNS Angiogenesis and Blood-Brain Barrier Integrity. *Circ. Res.* **127**, 466–482 (2020).
33. Bao, X. *et al.* Quantitative protein expression of blood-brain barrier transporters in the vasculature of brain metastases of patients with lung and breast cancer. *Clin. Transl. Sci.* **14**, 1265–1271 (2021).
34. Schaffenrath, J. *et al.* Blood-brain barrier alterations in human brain tumors revealed by genome-wide transcriptomic profiling. *Neuro-Oncol.* **23**, 2095–2106 (2021).
35. Cui, Y. *et al.* Brain endothelial PTEN/AKT/NEDD4-2/MFSD2A axis regulates blood-brain barrier permeability. *Cell Rep.* **36**, 109327 (2021).
36. Pilotto Heming, C. *et al.* P-glycoprotein and cancer: what do we currently know? *Heliyon* **8**, e11171 (2022).
37. Lu, T. M. *et al.* Pluripotent stem cell-derived epithelium misidentified as brain microvascular endothelium requires ETS factors to acquire vascular fate. *Proc. Natl. Acad. Sci.* **118**, e2016950118 (2021).

38. Duvivier, L., Gerard, L., Diaz, A. & Gillet, J.-P. Linking ABC transporters to the hallmarks of cancer. *Trends Cancer* **10**, 124–134 (2024).

39. Zhang, W. *et al.* Machine learning-based investigation of regulated cell death for predicting prognosis and immunotherapy response in glioma patients. *Sci. Rep.* **14**, 4173 (2024).

40. Lin, H.-H. *et al.* Overexpression of Cell-Surface Marker SLC16A1 Shortened Survival in Human High-Grade Gliomas. *J. Mol. Neurosci. MN* **71**, 1614–1621 (2021).

41. Cappoli, N., Jenkinson, M. D., Dello Russo, C. & Dickens, D. LAT1, a novel pharmacological target for the treatment of glioblastoma. *Biochem. Pharmacol.* **201**, 115103 (2022).

42. Kuan, C.-T. *et al.* MRP3: a molecular target for human glioblastoma multiforme immunotherapy. *BMC Cancer* **10**, 468 (2010).

43. Yan, Y., Liu, Y., Liang, Q. & Xu, Z. Drug metabolism-related gene ABCA1 augments temozolomide chemoresistance and immune infiltration abundance of M2 macrophages in glioma. *Eur. J. Med. Res.* **28**, 373 (2023).

44. Huang, J. *et al.* Application of blood brain barrier models in pre-clinical assessment of glioblastoma-targeting CAR-T based immunotherapies. *Fluids Barriers CNS* **19**, 38 (2022).

45. Herishanu, Y. *et al.* Activation of CD44, a receptor for extracellular matrix components, protects chronic lymphocytic leukemia cells from spontaneous and drug induced apoptosis through MCL-1. *Leuk. Lymphoma* **52**, 1758–1769 (2011).

46. Lai, Y. *et al.* Crosstalk between glioblastoma and tumor microenvironment drives proneural-mesenchymal transition through ligand-receptor interactions. *Genes Dis.* **11**, 874–889 (2024).

47. Wang, B. *et al.* IL-17 induces the proliferation and migration of glioma cells through the activation of PI3K/Akt1/NF-κB-p65. *Cancer Lett.* **447**, 93–104 (2019).

48. So, J.-S., Kim, H. & Han, K.-S. Mechanisms of Invasion in Glioblastoma: Extracellular Matrix, Ca2+ Signaling, and Glutamate. *Front. Cell. Neurosci.* **15**, (2021).

49. Takeuchi, H., Hashimoto, N., Kitai, R., Kubota, T. & Kikuta, K. Proliferation of vascular smooth muscle cells in glioblastoma multiforme. *J. Neurosurg.* **113**, 218–224 (2010).

50. Yan, T. *et al.* TGF-β induces GBM mesenchymal transition through upregulation of CLDN4 and nuclear translocation to activate TNF-α/NF-κB signal pathway. *Cell Death Dis.* **13**, 339 (2022).

51. Li, C.-W. *et al.* Epithelial–Mesenchymal Transition Induced by TNF-α Requires NF-κB–Mediated Transcriptional Upregulation of Twist1. *Cancer Res.* **72**, 1290–1300 (2012).

52. Guilhamon, P. *et al.* Single-cell chromatin accessibility profiling of glioblastoma identifies an invasive cancer stem cell population associated with lower survival. *eLife* **10**, (2021).

53. Farsi, Z. & Allahyari Fard, N. The identification of key genes and pathways in glioblastoma by bioinformatics analysis. *Mol. Cell. Oncol.* **10**, 2246657 (2023).

54. Iwadate, Y. Epithelial-mesenchymal transition in glioblastoma progression. *Oncol. Lett.* **11**, 1615–1620 (2016).

55. Smith, L. J. *et al.* Engineered In Vitro Tumor Model Recapitulates Molecular Signatures of Invasion in Glioblastoma. *ACS Mater. Au* **3**, 514–527 (2023).

56. Mammoto, T. *et al.* Role of collagen matrix in tumor angiogenesis and glioblastoma multiforme progression. *Am. J. Pathol.* **183**, 1293–1305 (2013).

57. Xia, S. *et al.* Tumor microenvironment tenascin-C promotes glioblastoma invasion and negatively regulates tumor proliferation. *Neuro-Oncol.* **18**, 507–517 (2016).

58. Yuan, Z. *et al.* Extracellular matrix remodeling in tumor progression and immune escape: from mechanisms to treatments. *Mol. Cancer* **22**, 48 (2023).

59. Payne, L. S. & Huang, P. H. The pathobiology of collagens in glioma. *Mol. Cancer Res. MCR* **11**, 1129–1140 (2013).

60. Phon, B. W., Bhuvanendran, S., Ayub, Q., Radhakrishnan, A. K. & Kamarudin, M. N. Identification of Prominent Genes between 3D Glioblastoma Models and Clinical Samples via GEO/TCGA/CGGA Data Analysis. *Biology* **12**, (2023).

61. Seo, S., Nah, S.-Y., Lee, K., Choi, N. & Kim, H. N. Triculture Model of In Vitro BBB and its Application to Study BBB-Associated Chemosensitivity and Drug Delivery in Glioblastoma. *Adv. Funct. Mater.* **32**, 2106860 (2022).

62. Testa, E., Palazzo, C., Mastrantonio, R. & Viscomi, M. T. Dynamic Interactions between Tumor Cells and Brain Microvascular Endothelial Cells in Glioblastoma. *Cancers* **14**, (2022).

63. Zheng, Q. *et al.* IL-17A promotes cell migration and invasion of glioblastoma cells via activation of PI3K/AKT signalling pathway. *J. Cell. Mol. Med.* **23**, 357–369 (2019).

64. Tung, Y.-T. *et al.* A 3D Bioprinted Human Neurovascular Unit Model of Glioblastoma Tumor Growth. *Adv. Healthc. Mater.* e2302831 (2024) doi:10.1002/adhm.202302831.

65. Liu, T. *et al.* PDGF-mediated mesenchymal transformation renders endothelial resistance to anti-VEGF treatment in glioblastoma. *Nat. Commun.* **9**, 3439 (2018).

66. Huang, M. *et al.* Wnt-mediated endothelial transformation into mesenchymal stem cell-like cells induces chemoresistance in glioblastoma. *Sci. Transl. Med.* **12**, (2020).

67. Choi, S.-H. *et al.* Tumour-vasculature development via endothelial-to-mesenchymal transition after radiotherapy controls CD44v6(+) cancer cell and macrophage polarization. *Nat. Commun.* **9**, 5108 (2018).

68. Obermeier, B., Daneman, R. & Ransohoff, R. M. Development, maintenance and disruption of the blood-brain barrier. *Nat. Med.* **19**, 1584–1596 (2013).

69. Dieterich, L. C. *et al.* Transcriptional profiling of human glioblastoma vessels indicates a key role of VEGF-A and TGFβ2 in vascular abnormalization. *J. Pathol.* **228**, 378–390 (2012).

70. Liddelow, S. A. & Barres, B. A. Reactive Astrocytes: Production, Function, and Therapeutic Potential. *Immunity* **46**, 957–967 (2017).

71. Perelroizen, R. *et al.* Astrocyte immunometabolic regulation of the tumour microenvironment drives glioblastoma pathogenicity. *Brain* **145**, 3288–3307 (2022).

72. Guan, X., Hasan, M. N., Maniar, S., Jia, W. & Sun, D. Reactive Astrocytes in Glioblastoma Multiforme. *Mol. Neurobiol.* **55**, 6927–6938 (2018).

73. Okolie, O. *et al.* Reactive astrocytes potentiate tumor aggressiveness in a murine glioma resection and recurrence model. *Neuro-Oncol.* **18**, 1622–1633 (2016).

74. Matias, D. *et al.* Microglia/Astrocytes-Glioblastoma Crosstalk: Crucial Molecular Mechanisms and Microenvironmental Factors. *Front. Cell. Neurosci.* **12**, 235 (2018).

75. Ma, J., Chen, C. C. & Li, M. Macrophages/Microglia in the Glioblastoma Tumor Microenvironment. *Int. J. Mol. Sci.* **22**, (2021).

76. Engler, J. R. *et al.* Increased Microglia/Macrophage Gene Expression in a Subset of Adult and Pediatric Astrocytomas. *PLOS ONE* **7**, e43339 (2012).

77. Ricci-Vitiani, L. *et al.* Tumour vascularization via endothelial differentiation of glioblastoma stem-like cells. *Nature* **468**, 824–828 (2010).

78. Soda, Y. *et al.* Transdifferentiation of glioblastoma cells into vascular endothelial cells. *Proc. Natl. Acad. Sci. U. S. A.* **108**, 4274–4280 (2011).

79. Viapiano, M. S., Bi, W. L., Piepmeier, J., Hockfield, S. & Matthews, R. T. Novel tumor-specific isoforms of BEHAB/brevican identified in human malignant gliomas. *Cancer Res.* **65**, 6726–6733 (2005).

80. Torrisi, F. *et al.* The Hallmarks of Glioblastoma: Heterogeneity, Intercellular Crosstalk and Molecular Signature of Invasiveness and Progression. *Biomedicines* **10**, (2022).

81. Pombero, A., Garcia-Lopez, R. & Martínez, S. Pericyte–Glioblastoma Cell Interaction: A Key Target to Prevent Glioblastoma Progression. *Cells* **12**, (2023).